



Characterisation of width-dependent diffusion dynamics in rubidium-exchanged KTP waveguides

LAURA PADBERG,^{1,*} MATTEO SANTANDREA,¹  MICHAEL RÜSING,² JULIAN BROCKMEIER,³ PETER MACKWITZ,³ GERHARD BERTH,³ ARTUR ZRENNER,³ CHRISTOF EIGNER,¹  AND CHRISTINE SILBERHORN¹ 

¹*Integrated Quantum Optics, Paderborn University, Warburger Strasse 100, 33098 Paderborn, Germany*

²*Institute of Applied Physics, Technical University Dresden, 01062 Dresden, Germany*

³*Nanostructure Optoelectronics, Paderborn University, Warburger Strasse 100, 33098 Paderborn, Germany*

*laura.padberg@uni-paderborn.de

Abstract: Integrated $\chi^{(2)}$ devices are a widespread tool for the generation and manipulation of light fields, since they exhibit high efficiency, a small footprint and the ability to interface them with fibre networks. Surprisingly, some commonly used material substrates are not yet fully understood, in particular potassium titanyl phosphate (KTP). A thorough understanding of the fabrication process of waveguides in this material and analysis of their properties is crucial for the realization and the engineering of high efficiency devices for quantum applications. In this paper we present our studies on rubidium-exchanged waveguides fabricated in KTP. Employing energy dispersive X-ray spectroscopy (EDX), we analysed a set of waveguides fabricated with different production parameters in terms of time and temperature. We find that the waveguide depth is dependent on their widths by reconstructing the waveguide depth profiles. Narrower waveguides are deeper, contrary to the theoretical model usually employed. Moreover, we found that the variation of the penetration depth with the waveguide width is stronger at higher temperatures and times. We attribute this behaviour to stress-induced variation in the diffusion process.

© 2020 Optical Society of America under the terms of the [OSA Open Access Publishing Agreement](#)

1. Introduction

Nonlinear waveguide structures are essential for state generation and manipulation and provide a compact solution for interfacing components of a quantum network operating at different wavelengths [1,2]. Moreover, waveguides offer stronger field confinement, thus achieving much higher efficiencies per unit length than their bulk counterparts. Among the different technological platforms like the well-known lithium niobate, KTP is especially interesting because it possesses unique dispersion properties which make it highly interesting for quantum state generation [3]. Nevertheless the behavior of KTP during waveguide fabrication and periodic poling is not fully understood. KTP offers large nonlinear optical and electro-optical coefficients [4], a wide transparency range extending well into the UV region [4], high damage thresholds and low photorefractive [5]. Moreover, its anisotropy of the domain growth facilitates the poling of the material [6], thus enabling the realization of sub-micron structures. Finally, the possibility to fabricate waveguides [7] makes this platform ideal for the development of integrated devices. For these reasons, the development of homogeneous waveguides in potassium titanyl phosphate is of great interest. However, waveguide structures are much more sensitive to inhomogeneities and fabrication imperfections, that can result in increased losses and reduced efficiency.

Several techniques have been used to produce waveguides in KTP, e.g. via ion-exchange (by channel diffusion [7], as well as in combination with dicing [8,9]) or laser writing [10]. Ridge waveguides offer a high mode confinement due to the substrate-air boundaries, but the losses

are rather high. They were measured to be not lower than 1.3dB/cm [8]. The most promising up-to-date technology makes use of rubidium-exchanged channel waveguides, as they have shown remarkably low losses of 0.67 dB/cm [11]. The fabrication is known to be non trivial [7], but no rigorous investigation of fabrication dynamics have been conducted so far. Using energy dispersive X-ray spectroscopy (EDX) we have analysed the concentration profiles of planar and channel Rb:KTP waveguides and characterized the diffusion profile of rubidium for different fabrication conditions. The EDX measurements have revealed an unexpected dependence of the diffusion depth to the waveguide width. With the help of Raman analysis, we show that this unusual dynamics can be related to stress present in the waveguide.

2. Waveguide fabrication and EDX methodology

For the waveguide profile analysis, we cut a commercially available flux grown single domain wafer (Bright Crystals Technology, Inc.) into smaller pieces of (10x6x1)mm along the crystallographic directions a-b-c. The optical quality of the a-b surface is specified to scratch dig 10-5. We fabricated waveguides in KTP by a rubidium-potassium exchange, which results in a local in-diffusion of rubidium in the KTP bulk material. The diffusion is highly anisotropic along the c-direction [12] and is induced by the one dimensional channels along this direction [4]. The rubidium increases the refractive index of the material which allows waveguiding in the in-diffused region [7]. The Rb-K exchange is performed by immersing the sample in a rubidium nitrate (RbNO₃), potassium nitrate (KNO₃) and barium nitrate (Ba(NO₃)₂) melt for a specific time and at a specific temperature. The used melt composition was chosen to be 97 mol% RbNO₃, 1 mol% Ba(NO₃)₂ and 2 mol% KNO₃ which allows for the reproducible fabrication of single mode waveguides at 1550nm. The samples were immersed with the a-b plane parallel to the melt surface.

The simplest description of rubidium in-diffusion consists in modelling the melt as an infinite reservoir for the diffusion process and assuming a concentration-independent diffusion coefficient D . The resulting concentration profile of the exchanged Rb ions follows a complementary error function [13]

$$c(z, t) = c_0 \cdot \operatorname{erfc} \left(\frac{z}{2 \cdot [D(T) \cdot t]^{1/2}} \right). \quad (1)$$

where c is the concentration of rubidium ions inside the crystal, c_0 is the surface concentration of rubidium, t is the exchange time and T is the temperature. Throughout the paper, we consider a reference frame with xyz aligned with the crystallographic axes a, b and c, respectively. The crystal extends in the region of space $z \geq 0$, where the plane $z = 0$ describes the top surface of the crystal, where exchange takes place, and the centre of the waveguide is located along the plane $y=0$.

Planar waveguides are produced by directly immersing the sample into the melt. To fabricate channel waveguides, a titanium mask is photolithographically patterned on the -c face of the KTP crystal. This is necessary to allow for optimal periodic poling of the bulk crystal prior waveguide fabrication in future samples. In the investigated samples, the channel width was varied from 1.5 μm to 4.5 μm . Prior to EDX and Raman measurements the end facets (b-c plane) of the samples were polished by chemical-mechanical polishing (CMP). This allows for an easier localization of the waveguides during the EDX measurements and it ensures a cleaner signal for the EDX and Raman measurements.

We determined the concentration profiles of the waveguides using EDX. For each waveguide, we measured ten times along a line on the end facet as shown in the inset of Fig. 1(a). In this way, we were able to retrieve the Rb concentration profile at the centre of the waveguide. The measured profile shows a trend compatible with the 1D diffusion model described above. The measured EDX data are a convolution of different process parameters such as the geometry of the excitation beam and effects due to the edge of the sample. For the determination of the concentration

profile, we convolute the expected complementary error function with a Gaussian and a Heaviside function and fit this to the measured data, see rose line in Fig. 1(a). The Heaviside function describes the edge of the sample. For the spread of the electron beam which has a Gaussian distribution, we exploit a gaussian function which describes a 220 nm wide excitation beam. The dark red line shows the deconvoluted complementary error function and the reconstructed rubidium concentration profile of a waveguide. From this reconstructed concentration profile we calculate the penetration depth that can be defined as $c(z, t)/c_0 = \text{erfc}(1)$, that is [14]

$$d = 2 \cdot [D(T) \cdot t]^{1/2}. \quad (2)$$

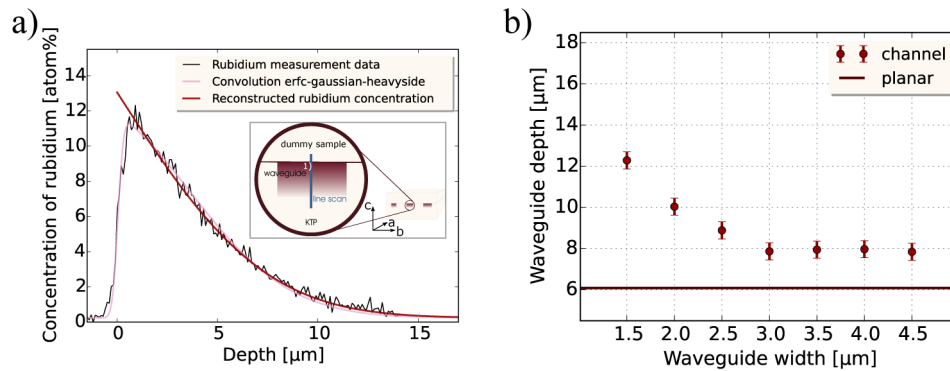


Fig. 1. a) Measured rubidium concentration in black and fit of the convolution of the expected complementary error, gaussian and Heaviside function in rose. The red line shows the reconstructed concentration profile and the calculated depth for a 3.0 μm channel waveguide. The inset shows how the waveguides have been measured. With a linescan at the b-c plane the concentration profile in depth has been reconstructed. b) Waveguide depth depending on the waveguide width of a sample produced at 330°C for 60 min. The dark red line shows the depth of planar waveguides produced at 330°C for 60 min. The offset between channel and planar waveguides cannot be explained with the current understanding of the diffusion process.

3. Waveguide analysis

We studied the diffusion properties and dynamics of Rb in KTP. For that we investigated the penetration depth of planar and channel waveguides produced at 330°C for 60 min. Using these parameters it is possible to fabricate waveguides, which guide only one mode at infrared wavelengths [11].

3.1. Energy dispersive X-ray spectroscopy

The results of the EDX measurements of planar and channel waveguides with different width are displayed in Fig. 1(b). Both waveguide types are fabricated with the same parameters. Comparing the penetration depths of channel waveguides and planar waveguides, one can see that the channel waveguides are at least 2 μm deeper even though both of them are produced with the same fabrication parameters. Moreover, we can clearly see a trend towards increasing waveguide depth with decreasing width of the waveguides. These observations clearly demonstrate that the simple model is not capable of describing the whole diffusion dynamics of Rb in KTP. The expected erfc function in Fig. 1(a) validates to assume a 1D model, but the model is not valid in comparison for different geometries in Fig. 1(b).

To investigate the nontrivial diffusion properties of KTP in more detail, we fabricated a new set of waveguides for 5 min at 330°C. The results of the comparison are shown in Fig. 2(a). Two main features can be recognized. Firstly, the diffusion depth in waveguides larger than 3.0 μm is not influenced by the diffusion time. This is in agreement with the result reported by Bierlein et al. [7]. Secondly, for short exchange times, the waveguide depths have a lower variability and seem uncorrelated with the waveguide widths. For getting a deeper understanding we also had a look at the surface concentration of the waveguides. In a simple model we assume an infinite reservoir for the exchanged waveguides and would expect the surface concentration to be independent of the exchange time. This would indicate that the surface concentration for 5 min and 60 min should be the same, but this is not the case. Figure 2(b) shows the ratio of exchanged potassium ions with rubidium ions $\frac{c_{Rb_0}}{c_{K_{mean}}}$ where c_{Rb_0} is the surface concentration of rubidium at the beginning of the waveguide. $c_{K_{mean}}$ is the mean value of the concentration of potassium inside the KTP bulk material analysed with a second linescan outside the waveguide. Therefore a completely exchanged surface has a ratio of 1. The 5 min exchanged waveguides have a mean ratio over all waveguide widths of 0.29 ± 0.03 , while the mean ratio of the 60 min exchanged waveguides with a value of 0.66 ± 0.06 is more than twice as high. We can also see that the surface concentration is independent of the waveguide width, even though the waveguide depth changes with the width. We attribute the width-dependent waveguide depth to the presence of stress in the transition area between KTP and rubidium-exchanged KTP. Stress can be expected due to the large lattice mismatch between KTP and rubidium titanyl phosphate (RTP) [15] since the rubidium ions are larger than the potassium ions. We expect that for small waveguides we will find more stress because these transition areas are located closer together. This stress could influence the diffusion properties and therefore the diffusion depth.

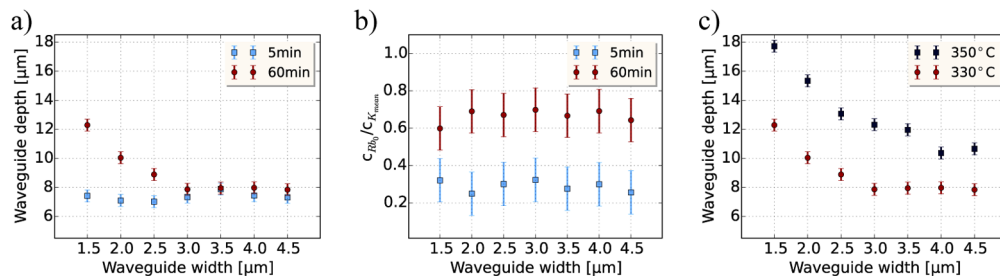


Fig. 2. a) Waveguide depth depending on the waveguide width of a sample produced at 330°C for 5 min (light blue) and 60 min (red) in 97 mol% RbNO₃, 1 mol% Ba(NO₃)₂, 2 mol% KNO₃. The uncertainty of the waveguide depth is calculated via standard deviation to $\pm 0.4 \mu\text{m}$. b) Ratio of exchanged potassium ions with rubidium ions at the surface depending on the waveguide width of a sample produced at 330°C for 5 min (light blue) and for 60 min (red) in 97 mol% RbNO₃, 1 mol% Ba(NO₃)₂, 2 mol% KNO₃. The uncertainty of the ratio is calculated to ± 0.12 . c) Waveguide depth depending on the waveguide width of a sample produced at 330°C for 60 min (red) and 350°C for 60 min (dark blue) in 97 mol% RbNO₃, 1 mol% Ba(NO₃)₂, 2 mol% KNO₃.

Furthermore, we produced a new sample with the same mask exchanged for 60 min at 350°C to see the influence of the temperature. In principle we would expect deeper waveguides with higher temperatures and that is exactly what we measured, as shown in Fig. 2(c). The waveguides produced at 350°C are deeper than the ones produces at 330°C. Moreover we can see that the trend of deeper waveguides with narrower widths is also present for higher temperatures.

Note that we have only analysed waveguides produced on the -c face. The diffusion profile will be different for waveguides produced on the +c face, as the diffusion properties change depending

on the crystal axis orientation [12]. This implies that the diffusion profile of periodically poled waveguides strongly depends on the local orientation of the domains [16].

EDX is only sensitive to the atomic stoichiometry, while it cannot provide any information on stress and other structural properties, e.g. disorder or defects. Raman spectroscopy can be used to search for exchange-induced stress as it was previously demonstrated [17–21].

3.2. Raman spectroscopy

To investigate the waveguide structures for stress, confocal Raman imaging has been performed on a set of waveguides with widths of 4.5 μm , 3.5 μm , 2.5 μm , and 1.5 μm and a control channel of 40 μm width, respectively. The Raman imaging was performed in a similar experimental geometry as the EDX measurements shown in Fig. 1. The incident light was focused on the a-surface and the scattered light was collected in backward direction through the same objective. The light polarization of the incident and detected light was parallel to the c-direction allowing for the detection of A_1 -TO phonons [22]. Examples of the Raman traces are shown in Fig. 3(c) and (d).

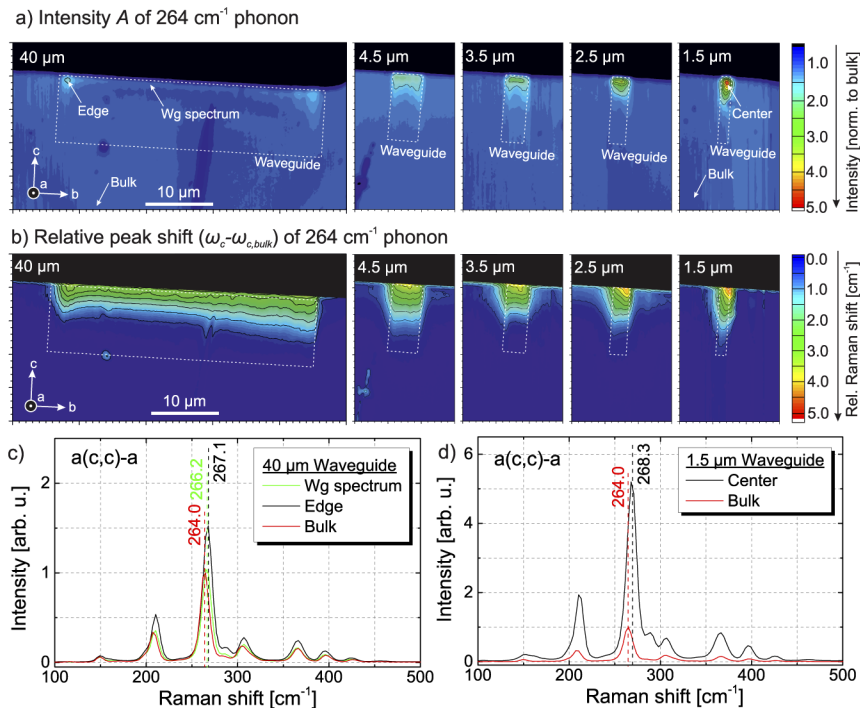


Fig. 3. Raman images for the control channel of 40 μm width and waveguides with width of 4.5 μm , 3.5 μm , 2.5 μm , and 1.5 μm visualized based on the (a) intensity and (b) the peak shift of the 264 cm^{-1} phonon. With decreasing waveguide width a progressively increasing intensity in the waveguide region is observed. This is also observed, when individual spectra of a (c) 40 μm control channel and (d) 1.5 μm waveguides are compared, which are taken at the locations highlighted in (a).

The Raman analysis performed here is based on the Lorentzian fit of the peak at 264 cm^{-1} using the following form

$$I(\omega) = \frac{A}{2\pi} \frac{\Gamma}{(\omega^2 - \omega_c^2) + \Gamma^2/2}. \quad (3)$$

Here, A corresponds to the intensity of the line, ω_c the peak center Raman shift, and Γ to the line width. This peak is associated with a vibration of the TiO_6 octahedron [23,24]. In RTP this line is observed at a slightly higher frequency compared to KTP at approximately 270 cm^{-1} [23,24], which can be explained by a compression of the TiO_6 octahedron due to the larger Rb ion radius [25,26]. The intensity of this line has been observed to be similar in both KTP and RTP, due to the similar electronic structure. Therefore, for the ion-exchanged region we expect the waveguide not to show a significant imprint in the spatial distribution of the intensity A . However, we do expect the exchanged region to be visible in the plot of the frequency ω_c of the chosen phonon. The obtained plots are shown in 3(a) and (b), respectively. The intensity in all plots was normalized to the surrounding bulk intensity, while the frequency shift is plotted as a relative shift, where the bulk value $\omega_{c,bulk} = 264.0\text{ cm}^{-1}$ was subtracted.

In the intensity plot of the $40\text{ }\mu\text{m}$ control channel the ion exchanged region shows no significant imprint on the phonon intensity in the center region of the waveguide, while only the waveguide edges are visible as several μm wide regions, where an intensity increase of up to $1.5\times$ compared to the surrounding bulk KTP is observed. In the bulk region surrounding the waveguides intensity variations of ± 0.25 are visible, which are due to local scattering of the pump, e.g. due to dust or microscopic scratches, which do not further affect the measurements. For smaller waveguides, the intensity in the waveguide region is progressively increasing with decreasing waveguide width. This is also seen when individual spectra from different locations are investigated. The approximate locations of the spectra are marked with an arrow. Figure 3(c) shows a spectrum from the center of the $40\text{ }\mu\text{m}$ control channel (green), which resembles the bulk KTP spectrum (red) in intensity and general structure, while only slight shifts of the bands are visible. This is expected when comparing bulk KTP and RTP spectra [23,24]. In contrast, the spectrum from the waveguide edge shows an increase in intensity over a broad spectral range and multiple phonons. This is more drastically seen for the $1.5\text{ }\mu\text{m}$ wide waveguide, where a more than $5\times$ increase in intensity is observed in the center of the waveguide. Stress can influence the scattering efficiency of Raman modes [27]. Due to the larger unit cell of RTP, the waveguides will experience stress. It is reasonable to assume that the stress is mostly localized at the interface between the exchanged waveguide and the pure bulk crystal and relaxes over a range of several μm as seen for the $40\text{ }\mu\text{m}$ control channel. Hence, it can be suspected that small waveguides will be progressively more strained, because the waveguides are smaller than the suspected relaxation range.

Similar conclusions can be made based on the plots of the relative peak shift in Fig. 3(b). For the $40\text{ }\mu\text{m}$ wide control channel in Fig. 3(b) the ion-exchanged region is visible as a region with increased peak wavenumber. The depth dependence in the center of this waveguide approximately resembles a diffusion profile comparable to the EDX profiles with progressively increased frequency towards the surface. However, phonon frequencies are also influenced by other parameters, such as stress. This is particularly visible for the smaller waveguides. Here, the region which shows an increased frequency is larger than the waveguide width, i.e. the region of the ion exchange. Especially for the smaller waveguides the region of increased intensity extends several μm over the waveguide borders. The increase in frequency in this region indicates a compressive strain component [28], which is expected due to the larger unit cell size of RTP. To reconstruct diffusion profiles from Raman spectroscopy, further analysis is necessary to distinguish strain and composition related effects. A potential pathway can be the investigation of (unstrained) bulk mixed crystals of different compositions, as well as theoretical studies of the Raman spectra by ab-initio methods as shown for other ferroelectrics [29,30].

In conclusion, the Raman investigation indicate that the waveguides in the range $1.5\text{ }\mu\text{m}$ - $4.5\text{ }\mu\text{m}$ are increasingly affected by the stress with decreasing waveguide width and thus the diffusion dynamic inside the waveguide is poorly modeled by Eq. (1).

4. Simulations

Seeing that the measured stress from the Raman spectroscopy shows unique behaviour for narrow and broad waveguides, we investigate if a stress-dependent diffusion coefficient can explain the data reported in Fig. 2. A reasonable assumption is to connect the diffusion coefficient D to the local concentration of Rb in the crystal, as a higher Rb content results in a greater distortion of the crystalline lattice. For simplicity, we assume an exponential dependence of the diffusion coefficient D on the concentration c of Rb

$$D(c) = D_0 \cdot \exp [k(y) \cdot c(z)]. \quad (4)$$

The parameter k is related to the amount of stress that is present locally: higher stress is associated to a higher value of k , such that the diffusion is more affected by the Rb concentration.

Equation (4) assumes that the whole waveguide is characterized by the same level of stress k . However, the Raman measurements show that stress is localized nearby the edge of the waveguide, and is gradually relaxed over 2-3 μm . We can model this observation assuming a spatially varying k , which is maximum at the edges of the waveguide and decays towards $k = 0$ (in the limit of large waveguide width) at the centre of the waveguide. A possible function that models this behaviour is

$$k(y) = k_0 \left[1 + \frac{1}{2} \operatorname{erf} \left(\frac{y - \frac{w}{2}}{\sigma} \right) - \frac{1}{2} \operatorname{erf} \left(\frac{y + \frac{w}{2}}{\sigma} \right) \right], \quad (5)$$

where $y = 0$ corresponds to the centre of the waveguide and w is the waveguide width. The parameter σ determines how quickly stress is relaxed towards the centre of the waveguide, while k_0 determines the strength of the stress at the edges of the waveguide.

The model has three free parameters, D_0 , k_0 and σ . We set $D_0 = 0.25 \mu\text{m}^2/\text{min}$ in order to match the waveguide depths for the wider waveguides, since their constant depths suggest that stress has little impact in these structures ($k = 0$). From the Raman measurements, we set $\sigma = 1 \mu\text{m}$, as we have seen that the stress is relaxed over such distance.

We follow the method presented in [31] to solve the diffusion equation with a concentration-dependent D . Since the EDX data are taken at the centre of the waveguide, we calculate the diffusion profile by evaluating k at $y = 0$ from Eq. (5) and solving the diffusion equation with $D = D_0 \exp [k(0)c]$.

We optimize the parameter k_0 to match the measured and the simulated depth of the waveguides, for different nominal widths. The comparison between simulations with $k_0=3.1$ and the measured data is shown in Fig. 4. Note that the values of k_0 , D_0 and σ are valid only for the diffusion process discussed in this paper.

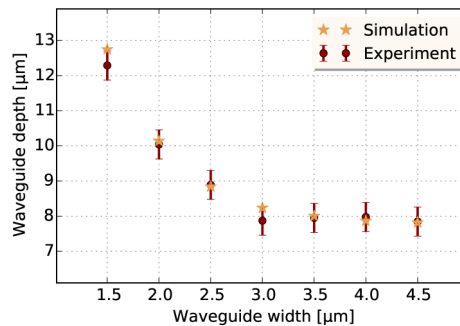


Fig. 4. Simulations with stress-dependent diffusion coefficients displays the trend of deeper diffusion depth with narrower waveguide width.

A few comments are necessary regarding the presented model. The relationship between the Rb concentration, the stress in the waveguide and the diffusion coefficient provided in Eqs. (4) and 5 have been chosen to be physically reasonable, but their real interplay is still unknown. Moreover, this model cannot reproduce the measurements for the 5 min-diffused waveguides. In fact, it can be shown that, if the D depends only on the Rb concentration, it is impossible to have identical diffusion depths for a 5 min and a 60 min diffusion [31]. This suggests that the overall diffusion process in our waveguide structures changes over time. We speculate that the diffusion process consists of at least two successive steps. In the first step, which lasts approximately for the first 5 min of the exchange, the diffusion is fast and stress is not critical in determining the concentration profile. In the second step, the overall diffusion slows down but, at the same time, stress starts becoming more relevant, thus determining a width-dependent diffusion depth.

Further measurements are needed to validate our speculations and improve the modelling. It will be important to characterize the waveguide depths and the Raman images of waveguides fabricated with diffusion times ranging from a few minutes to a few hours. This will help understanding whether the build-up of the stress is a long term dynamics or if it arises already in the first minutes of the diffusion, and it will help to map the time evolution of the diffusion coefficient. Finally, it is necessary to characterise the concentration profile at different positions within the waveguide cross section, to monitor how much the presence of the stress nearby the waveguide edge affects the diffusion. Unfortunately, EDX is not particularly suited for this purpose, since the minimum dimensions of the interaction volume prevent the resolution of features smaller than $\sim 1.4 \mu\text{m}$. Only with these additional measurement it will be possible to improve our understanding of the highly nonlinear diffusion of Rb into KTP.

5. Conclusion

In conclusion, we have characterized for the first time methodically the diffusion process for the realization of rubidium-exchanged waveguides in KTP. We were able to show that the penetration depth depends on the width of the waveguide. We find that the narrower we produce our waveguides the deeper they become in comparison to a simple one dimensional diffusion model. Moreover one can see that the variation of the penetration depth with the width is stronger for higher temperatures and longer diffusion times. Our preliminary Raman analysis reveals the presence of stress, in particular at the edge of the waveguides. This is likely to modify the diffusion dynamics of Rb and could explain the breakdown of the simple 1D diffusion model. The underlying mechanisms, however, are not fully understood yet and further analysis, e.g. Raman spectroscopy or SHG microscopy, is necessary.

This work shows complex rubidium-exchange behaviour needs further investigations for a complete explanation of the empirical observations. But the first Raman measurements suggest that stress in the waveguide might be a critical factor in the diffusion process. Further understanding of these effects will be crucial for the realization of improved waveguide performance in this material. A more complete understanding of the rubidium-exchange process will enable the fabrication of more homogeneous and uniform KTP waveguides.

Funding

Deutsche Forschungsgemeinschaft (Projektnummer 231447078, SFB - TRR 142).

Acknowledgments

Funded by the Deutsche Forschungsgemeinschaft (DFG, German Research Foundation) - Projektnummer 231447078 - TRR 142.

Disclosures

The authors declare no conflicts of interest.

References

1. N. Maring, P. Farrera, K. Kutluer, M. Mazzera, G. Heinze, and H. de Riedmatten, "Photonic quantum state transfer between a cold atomic gas and a crystal," *Nature* **551**(7681), 485–488 (2017).
2. H. Rütz, K.-H. Luo, H. Suche, and C. Silberhorn, "Quantum frequency conversion between infrared and ultraviolet," *Phys. Rev. Appl.* **7**(2), 024021 (2017).
3. G. Harder, V. Ansari, B. Brecht, T. Dirmeier, C. Marquardt, and C. Silberhorn, "An optimized photon pair source for quantum circuits," *Opt. Express* **21**(12), 13975 (2013).
4. J. Bierlein and H. Vanherzeelen, "Potassium titanyl phosphate: properties and new applications," *J. Opt. Soc. Am. B* **6**(4), 622 (1989).
5. D. T. Chu, H. Hsiung, L. K. Cheng, and J. D. Bierlein, "Curie temperature and dielectric properties of doped and undoped KTiOPO_4 and isomorphs," *IEEE Trans. Ultrason., Ferroelect., Freq. Contr.* **40**(6), 819–824 (1993).
6. C. Canalias, J. Hirohashi, V. Pasiskevicius, and F. Laurell, "Polarisation-switching characteristics of flux-grown KTiOPO_4 and rbitiopo_4 at room temperature," *J. Appl. Phys.* **97**(12), 124105 (2005).
7. J. Bierlein, A. Ferretti, L. H. Brixner, and W. Hsu, "Fabrication and characterization of optical waveguides in KTiOPO_4 ," *Appl. Phys. Lett.* **18**, PDP5 (1987).
8. M. F. Volk, C. E. Rüter, M. Santandrea, C. Eigner, L. Padberg, H. Herrmann, C. Silberhorn, and D. Kip, "Fabrication of low-loss rb-exchanged ridge waveguides in z-cut KTiOPO_4 ," *Opt. Mater. Express* **8**(1), 82–87 (2018).
9. C. Eigner, M. Santandrea, L. Padberg, M. F. Volk, H. H. C. E. Rüter, D. Kip, and C. Silberhorn, "Periodically poled ridge waveguides in KTP for second harmonic generation in the UV regime," *Opt. Express* **26**(22), 28827–28833 (2018).
10. F. Laurell, T. Calmano, S. Müller, P. Zeil, C. Canalias, and G. Huber, "Laser-written waveguides in KTP for broadband type II second harmonic generation," *Opt. Express* **20**(20), 22308–22313 (2012).
11. V. Ansari, E. Roccia, M. Santandrea, M. Doostdar, C. Eigner, L. Padberg, I. Gianani, M. Sbroscia, J. M. Donohue, L. Mancino, M. Barbieri, and C. Silberhorn, "Heralded generation of high-purity ultrashort single photons in programmable temporal shapes," *Opt. Express* **26**(3), 2764–2774 (2018).
12. R. Wellendorf, C. Kaps, and R. Kriegel, "On the Rb^+ and K^+ counterdiffusion in single crystals of $\text{K}(\text{TiO})\text{PO}_4$ - a quasi-one-dimensional superionic conductor," *Ionics* **2**(3-4), 222–230 (1996).
13. J. Crank, "A theoretical investigation of the influence of molecular relaxation and internal stress on diffusion in polymers," *J. Polym. Sci.* **11**(2), 151–168 (1953).
14. Y. N. Korkishko and V. Fedorov, *Ion exchange in single crystals for integrated optics and optoelectronics* (Gordon and Breach Science Pub., Cambridge International Science Publishing, 1999).
15. F. C. Zumsteg, J. D. Bierlein, and T. E. Gier, " $\text{K}_x\text{Rb}_{1-x}\text{TiOPO}_4$: A new nonlinear optical material," *J. Appl. Phys.* **47**(11), 4980–4985 (1976).
16. C. Eigner, M. Santandrea, and C. Silberhorn, *Herstellung von Wellenleitern aus Materialien der KTP-Familie/Fabrication of waveguides from materials of the KTP family* (Patent number DE 10 2018 108 636.9, 2018).
17. O. Pea-Rodriguez, J. Olivares, M. Carrascosa, N. Garca-Cabaes, A. Rivera, and F. Agulló-López, *Ion Implantation* (InTech, 2012).
18. M. R. Tejerina, D. Jaque, and G. A. Torchia, "A 2D μ -raman analysis of low repetition rate femto-waveguides in lithium niobate by using a finite element model," *Opt. Mater.* **36**(5), 936–940 (2014).
19. I. DeWolf, H. E. Maes, and S. K. Jones, "Stress measurements in silicon devices through Raman spectroscopy: Bridging the gap between theory and experiment," *J. Appl. Phys.* **79**(9), 7148–7156 (1996).
20. I. DeWolf, "Stress measurements in si microelectronics devices using raman spectroscopy," *J. Raman Spectrosc.* **30**(10), 877–883 (1999).
21. M. Panlova, A. Pawlis, C. Arens, S. M. de Vasconcellos, G. Berth, K. Hüsich, V. Wiedemeier, A. Zrenner, and K. Lischka, "Micro-Raman imaging and micro-photoluminescence measurements of strain in $\text{ZnMgSe}/\text{ZnSe}$ microdiscs," *Microelectron. J.* **40**(2), 221–223 (2009).
22. M. Rüsing, C. Eigner, P. Mackwitz, G. Berth, C. Silberhorn, and A. Zrenner, "Identification of ferroelectric domain structure sensitive phonon modes in potassium titanyl phosphate: A fundamental study," *J. Appl. Phys.* **119**(4), 044103 (2016).
23. G. E. Kugel, F. Brèhat, B. Wyncket, M. D. Fontana, G. Marnier, C. Carabatos-Nedelec, and J. Mangin, "The vibrational spectrum of a KTiOPO_4 single crystal studied by Raman and infrared reflectivity spectroscopy," *J. Phys. C: Solid State Phys.* **21**(32), 5565–5583 (1988).
24. G. H. Watson, "Polarized Raman spectra of KTiOPO_4 and isomorphic nonlinear-optical crystals," *J. Raman Spectrosc.* **22**(11), 705–713 (1991).
25. N. I. Sorokina and V. I. Voronkova, "Structure and properties of crystals in the potassium titanyl phosphate family: A review," *Crystallogr. Rep.* **52**(1), 80–93 (2007).

26. P. A. Thomas, S. C. Mayo, and B. E. Watts, "Crystal structures of RbTiOAsO_4 , $\text{KTiO}(\text{P}_{0.58}\text{As}_{0.42})\text{O}_4$, RbTiOPO_4 and $(\text{Rb}_{0.465}\text{K}_{0.535})\text{TiOPO}_4$, and analysis of pseudosymmetry in crystals of the KTiOPO_4 family," *Acta Crystallogr., Sect. B: Struct. Sci.* **48**(4), 401–407 (1992).
27. M. D. Fontana, R. Hammoum, P. Bourson, S. Margueron, and V. Y. Shur, "Raman micro-spectroscopy as a probe to investigate ppln structures," *Ferroelectrics* **352**(1), 106–110 (2007).
28. G. A. Kourouklis, A. Jayaraman, A. A. Ballman, and M. Hill, "A high pressure Raman study of KTP and pressure induced phase transition," *Solid State Commun.* **62**(6), 379–382 (1987).
29. S. Sanna, S. Neufeld, M. Rüsing, G. Berth, A. Zrenner, and W. G. Schmidt, "Raman scattering efficiency in LiTaO_3 and LiNbO_3 crystals," *Phys. Rev. B* **91**(22), 224302 (2015).
30. M. Rüsing, S. Sanna, S. Neufeld, G. Berth, W. G. Schmidt, A. Zrenner, H. Yu, Y. Wang, and H. Zhang, "Vibrational properties of $\text{LiNb}_{1-x}\text{Ta}_x\text{O}_3$ mixed crystals," *Phys. Rev. B* **93**(18), 184305 (2016).
31. J. Crank, *The Mathematics of Diffusion* (Clarendon, 1975).